Histol Histopathol (2016) 31: 403-413

http://www.hh.um.es

Histology and Histopathology

From Cell Biology to Tissue Engineering

Development, differentiation, and vascular components of subcutaneous and intrahepatic Hepa129 tumors in a mouse model of hepatocellular carcinoma

Richard T. Robertson[1,3], Paula M. Gutierrez[1], Janie L. Baratta[1], Kristoffer Thordarson[1], Joshua Braslow[1], Sherry M. Haynes[2] and Kenneth J. Longmuir[2,3]

[1]Department of Anatomy and Neurobiology, [2]Department of Physiology and Biophysics and [3]The Chao Family Cancer Center, School of Medicine, University of California, Irvine, CA, USA

Summary. Tumor models in mice offer opportunities for understanding tumor formation and development of therapeutic treatments for hepatocellular carcinoma. In this study, subcutaneous or intra-hepatic Hepa129 tumors were established in C3H mice. Tumor growth was determined by daily measurements of subcutaneous tumors and post-mortem studies of subcutaneous and intrahepatic tumors. Administration of Edu was used to determine cell generation dates of tumor cells. Immunohistochemistry with antibodies directed at CD31 or CD34, and intravenous injection of labeled tomato lectin revealed tumor vasculature. Tissue sections also were processed for immunohistochemistry using a panel of antibodies to proteoglycans. Comparison of Edu labeled cells with immunoreactivity allowed determination of development and differentiation of tumor cells after cell generation.

Subcutaneous and intrahepatic tumors displayed similar growth over 3 weeks. Immunohistochemistry showed strong labeling for glypican-3, 9BA12, and chondroitin sulfate of tumors in both loci, while normal liver was negative. Tumor regions containing Edu labeled cells did not show significant immunohistochemical labeling for the tumor markers until 2-3 days after Edu treatment; overlap of Edu labeled cells and immunohistochemically labeled tumor regions appeared to reach a maximum at 5 days after Edu treatment. Ectopic subcutaneous tumors displayed vascular ingrowth as the tumor cells expressed immunocytochemical markers; subcutaneous tumors displayed significantly more vascular elements than did intrahepatic tumors.

Key words: Chondroitin sulfate, Edu labeling, Glypican-3, Proteoglycan, Vascular labeling

Offprint requests to: Richard T. Robertson, Department of Anatomy and Neurobiology, School of Medicine, University of California, Irvine, CA 92697-1280, USA. e-mail: rtrobert@uci.edu

DOI: 10.14670/HH-11-683

Introduction

Hepatocellular carcinoma (HCC) is a common cancer worldwide, and its frequency of occurrence has increased markedly in the past two decades (Forner et al., 2012). Unfortunately, HCC is resistant to treatment by irradiation or by current techniques of chemotherapy, and thus improved treatment methods, based upon increased understanding of the cell and tissue biology of HCC, are vitally important. Much attention is being focused on therapeutic strategies based on blocking angiogenesis into the newly formed tumors, so an understanding of the development of vascular growth into tumors is of particular interest.

Advances in understanding of HCC are facilitated by studies using animal models, due to the advantage of size, ease of maintenance, and the availability of genetic engineering (Leenders et al., 2008; Li et al., 2012; Bakiri and Wagner, 2013; DeMincis et al., 2013; Khaled and Liu, 2014). Syngeneic transplant models, in which small blocks of tissue or dissociated cells from tumors are surgically implanted into host mice, are of particular interest. A variety of tumor cell lines have been introduced (Heindryckx et al., 2009; Shiraha et al.,

2013), and a particularly attractive syngeneic implantation model of HCC is the Hepa129 system (Schmitz et al., 2004). This tumor can be established successfully ectopically (typically subcutaneously) and orthotopically (within the liver) in immunocompetent C3H mice. In our laboratory, we have examined glycosaminoglycans and proteoglycans that are expressed by Hepa129 cells, and found significant changes in chondroitin sulfate levels, chondroitin disaccharide compositions, and chondroitin proteoglycan expression compared to normal liver (Longmuir et al., 2015, unpublished data).

In the present study, we examined the development, differentiation, and vascularization of Hepa129 tumors stemming from transplantation of Hepa129 cells, either subcutaneously or intrahepatically, into C3H laboratory mice.

Materials and methods

Cell culture

Hepa129 tumor (Hepatoma 129) was obtained from the National Cancer Institute, Division of Cancer Treatment and Diagnosis (NCI-DCTD) Tumor Repository (Frederick, MD, USA). A portion of the tumor (approximately 0.2-0.3 cm each dimension) was rinsed with dissociation buffer, minced thoroughly, and then dissociated with 4 mL 0.05% trypsin in dissociation buffer in a 60 mm dish. After the majority of the tissue had dispersed into individual cells, the cells were centrifuged and the pellet suspended in Eagle minimum essential medium with 10% fetal calf serum and with antibiotic. The cells were maintained in this culture medium in 100 mm dishes, in a humidified incubator, with 5% CO_2, at 37°C.

Cells were pelleted by centrifugation and split 1:4 every two to three days. After 8 days, the culture dishes contained an apparently homogenous population of cells that exhibited spherical but otherwise featureless characteristics when viewed with phase contrast microscopy. The cells were loosely aggregated in suspension, remained unattached to the substrate, and readily dispersed into individual cells upon pipetting. Cells typically reached a density of $10x10^6$ per 100 mm dish prior to passing, and prior to *in vivo* injection.

Animals, tumor initiation and tumor harvest

Animal studies used female C3H mice (Charles River Laboratories), 18-25 g. The *in vivo* protocols were reviewed and approved by the University of California, Irvine, Institutional Animal Care and Use Committee (IACUC) prior to conducting the experiments. All research adhered to the ''Principles of Laboratory Animal Care'' (NIH publication #86-23, revised in 1985).

Approximately $10x10^6$ Hepa129 cells were pelleted, rinsed with Eagle MEM medium without serum and without antibiotic, counted, and re-suspended in this medium at a density of $5x10^6$ cells/ml. Animals were injected with 50 μl suspension containing $2.5x10^5$ cells. Subcutaneous injections were made under the skin of dorsal thorax. For liver injections, animals were anesthetized Ketamine/Xylazine (80 mg/kg Ketamine; 10 mg/kg Xylazine; IP). Surgical incisions of skin on the ventral midline, and through the anterior body wall, were made using aseptic precautions. The liver was exposed, and 50μl of cell suspension was infused over 15-20 sec into the left lateral lobe of the liver. As the injection needle was being withdrawn, a small piece of Gelfoam (Pharmacia and Upjohn, North Peapack NJ, USA) was placed at the injection site to retard effusion of tumor cells (Yang et al., 1992). Incisions in the muscles of the body wall and in the skin were sutured separately. Animals received subcutaneous injections of 30μl buprenorphine, were kept warm and turned at 15 min intervals, and were returned to the home cage when they recovered normal motility.

All animals were monitored daily for tumor development. Subcutaneous tumors were measured with calipers to obtain two perpendicular diameters, and volume estimated as $V=4/3\ \pi\ D_1/2xD_2/2xD_3/2$, with D_1 being the long diameter of the measured tumor and D_2 being the short diameter. The thickness of the tumor, as would be measured from the body wall externally, was difficult to determine from live animal measurements. Our post-mortem measurements of tumor sizes indicated that this third dimension ranged from approximately 3 mm to 5 mm over the post-injection time period; the third value D_3 contributing to the determination of tumor volume was set at 3 mm for any palpable tumor up to day 7 of tumor growth, 4 mm for any tumor from day 8 to day 14, and 5 mm for any tumor after day 14.

Animals were euthanized and tumors harvested between 7 and 21 days after injections. Mice were anesthetized with sodium pentobarbital (100mg/kg, i.p.), then perfused through the heart first with 10 ml of 0.9% saline and then with 20 ml of 4% paraformaldehyde, using a perfusion pump set at a flow rate of 5 ml/min. Liver and subcutaneous tumor were removed and placed in 4% paraformaldehyde overnight and then into 30% sucrose in Na-PO_4 buffered saline prior to freezing for cryostat sectioning.

Subcutaneous Hepa129 tumors and liver (both normal and tumor-bearing) were post-fixed in 4% paraformaldehyde and stored in 30% sucrose solution at 4°C for cryo-protection. Tissue sections were cut using a Reichert-Jung cryostat, at thickness 10-12 μm, and mounted directly onto prepared slides (Superfrost Plus slides; Fisher Scientific, Pittsburgh PA).

Vascular labeling studies

Intravenous injection of biotin- or fluorescent-labeled tomato lectin (*Lycopersicon esculentum*

agglutinin, Vector Labs, Burlingame CA), 100 μl at 1 mg/ml, were made into the tail vein of 8 mice with tumors, as described previously (Robertson et al., 2015). Following post-injection times of 5-10 min, animals were euthanized by vascular perfusion as described above. Fluorescently labeled lectin required no further processing to visualize the vasculature of tumors. Tissue from animals injected with the biotinylated lectin were processed using the Elite ABC Kit (Vector Labs; Burlingame CA). Both the biotinylated and fluorescently tagged lectin labeling procedures were compatible with Edu and immunohistochemical procedures as described below.

Edu studies

Times of tumor cell generation, determined by last DNA synthesis prior to mitotic cell division, were studied using the Edu protocol (Click-IT; Life Technologies, Grand Island NY). The Edu (5-ethynyl-2'-deoxyuridine, a nucleoside analog of thymidine) was prepared in saline at 2.5 mg/ml, and administered by IP or IV injections at 250 μg/100 μl for a 20 - 25 gram mouse. Following post-injection survival times ranging from 2 hr to 7 days, animals were anesthetized with sodium pentobarbital (100 mg/kg; IP) and perfused through the heart with a saline flush followed by 4% paraformaldehyde, as described above. Incorporated Edu leading to cell labeling was detected using a Click-IT Edu kit (Life Technologies, Grand Island NY). Either green (Alexa Fluor 488) or red (Alexa Fluor 594) fluorphores were used. When tissue sections were double labeled with Edu and immunocytochemistry, the immuncytochemistry was performed first, followed by the Edu processing.

Immunohistochemistry

Tumor tissue was studied using a variety of antibodies as listed in Table 1. Sections were rinsed in Tris buffer (0.1 M; pH 7.4) for 5 min and processed for nonspecific blocking in 3% normal goat serum for 1 hr. When using mouse IG's on mouse tissue, the tissue was first treated (30 min) with Fab fragments (Jackson Labs), to reduce non-specific binding by the anti-mouse secondary antibodies. Primary antibodies were diluted in Tris buffer (dilutions 1:10 to 1:500), placed onto the tissue slides, and incubated overnight at room temperature. Slides were rinsed 3x in Tris buffer and then incubated in secondary antibody for 2 hr at room temperature in darkness. The anti-albumin antibody was labeled with fluorescein, and required no secondary antibody. For the other primary antibodies, secondary antibodies included goat anti-rabbit, anti-rat, and anti-mouse, labeled with Alexa 488 or Alexa 594, and anti-mouse IgM labeled with Alexa 488 or Alexa 594. After incubation in the secondary antibody, slides were rinsed 3 times for 10 min each in Tris buffer, and then coverslipped with Vectashield (Vector labs, Burlingame CA). In most cases the Vectashield contained DAPI, a nuclear label visible under ultraviolet illumination.

Analyses

Tissue sections were inspected using a Nikon fluorescence microscope equipped with rhodamine, fluorescein, and ultraviolet filter sets. Images were captured using a Nikon DS 5M digital camera. To facilitate comparison of labeling intensity between sections, manually adjusted exposure parameters were used to ensure that photographic exposure parameters remained consistent. Images were imported into PhotoShop (Adobe Photoshop CS5.1; Adobe Systems, Mountain View CA). Comparisons of regions of tissue labeled by Edu and by immunohistochemistry were done using Photoshop areal measurements. Statistical analyses were accomplished using Student t-tests and Analysis of Variance (ANOVA), with the aid of GraphPad InStat and Exel software packages. The InStat ANOVA analyses were followed by Tukey-Kramer multiple comparison

Table 1. Antibodies used in immunohistochemical studies.

Name	Type	Dilution	Species	Supplier
Chondroitin Sulfate Proteoglycan, 9BA12	IgM	1:100	mouse	U Iowa Hybridoma Bank
Glypican-3	Polyclon	1:100	rabbit	Novus Biologicals
Glypican-1	antisera	1:100	rabbit	Novus Biologicals
Chondrotin Sulfate, CS-56	monoclon	1:100	mouse	Sigma-Aldrich or Abcam
Collagen IX, 2B9	IgM	1:100	mouse	U Iowa Hyrbridoma Bank
Heparan Sulfate	monoclon	1:100	rat	AbCam
Versican,12C5	IgG	1:100	mouse	U Iowa Hybridoma Bank
Decorin,3B3	IgG	1:100	bovine	U Iowa Hybridoma Bank
Albumin	IgG	1:500	goat	Bethyl Labs
CD34	IgG monoclon	1:100	mouse	Vector Labs
CD34	IgG	1:100	rabbit	AbCam.
CD31	IgG	1:100	rat	HistoBioTech

tests or Student t-tests.

Results

Growth of tumors

A total of 76 C3H mice received subcutaneous injections of Hepa129 tumor cells. Of these 76 mice, 35 mice also received injections of Hepa129 cells directly into the liver. Seventy of the 76 mice (92%) developed subcutaneous tumors; 4 of these mice died before they were euthanized by perfusion; 28 of the 35 mice with intrahepatic injections (80%) developed intrahepatic tumors. Subcutaneous tumors were solid, with a whitish nodular appearance. Intrahepatic tumors were recognized by their white nodular appearance beneath the liver capsule against the reddish brown of adjacent normal liver tissue.

Fig. 1A presents the growth pattern for the ectopic subcutaneous tumors as a function of time after injection. Measurements of tumor diameters were taken through the skin using calipers *in vivo*. No evidence of tumors was detected for the first several days following injection. After tumors became palpable at about day 5, growth was rapid. Maximal tumor volume appeared to be reached by 16 days after injection, and most animals were euthanized by this date. In animals maintained beyond 16 days, measurements of tumors were more variable and the tumors, as well as regions of the skin overlying the tumors, showed evidence of necrosis. No differences were detected in the rate of tumor growth or the size of tumors in animals that had only subcutaneous tumors compared to animals that had both subcutaneous and hepatic tumors.

Fig. 1B compares calculated volumes of tumors taken by calipers through the skin of living animals at days 12-14 after tumor cell transplantation, and of measurements of the tumors after perfusion fixation and excision. Results from a paired t-test demonstrate that the measurements taken *in vivo* over-estimate the tumor volume by about 29%, a difference that is statistically significant ($t=8.25$, $p<0.0001$)

Sizes of hepatic tumors were assessed after vascular perfusion and liver removal. As with subcutaneous tumors, diameters of the tumors were taken in three dimensions, but while subcutaneous tumors usually had an ovoid structure, the intrahepatic tumors were more irregular, and measurements more variable. The third histogram bar in fig. 1B presents data for calculated volumes of hepatic tumors taken at 12-14 days after tumor cell implantation. These data indicate that for animals that had both subcutaneous and intrahepatic tumors, the subcutaneous tumors were significantly larger ($t=2.78$, $p=0.0147$).

Immunohistochemical characteristics of tumors

Tumor tissue from mice euthanized at 8-18 days after injection of tumor cells was studied immunohistochemically. Fig. 2 presents representative photomicrographs showing immunoreactivity of intrahepatic tumors and subcutaneous tumors to 3 antibodies, in animals euthanized 12 days following tumor cell transplant. The top row of photomicrographs is taken of a series of cryostat sections showing an ovoid intrahepatic tumor, bordered by relatively normal liver tissue (Baratta et al., 2009). Immunoreactivity for glypican 3 (Gly-3; an antibody commonly used to identify human hepatocellular carcinoma; (Filmus and Capurro, 2013) is seen clearly in 2A, while normal liver tissue bordering the tumor appears Gly-3 negative. Similar patterns of immunoreactivity are seen when employing an antibody to chondroitin sulfate (CS-56) (Fig. 2B), or 9BA12 (Fig. 2C). Comparable photomicrographs of immunoreactivity in sections from subcutaneous tumors are presented in Fig. 2D-F. The subcutaneous tumors do not appear to be homogenous,

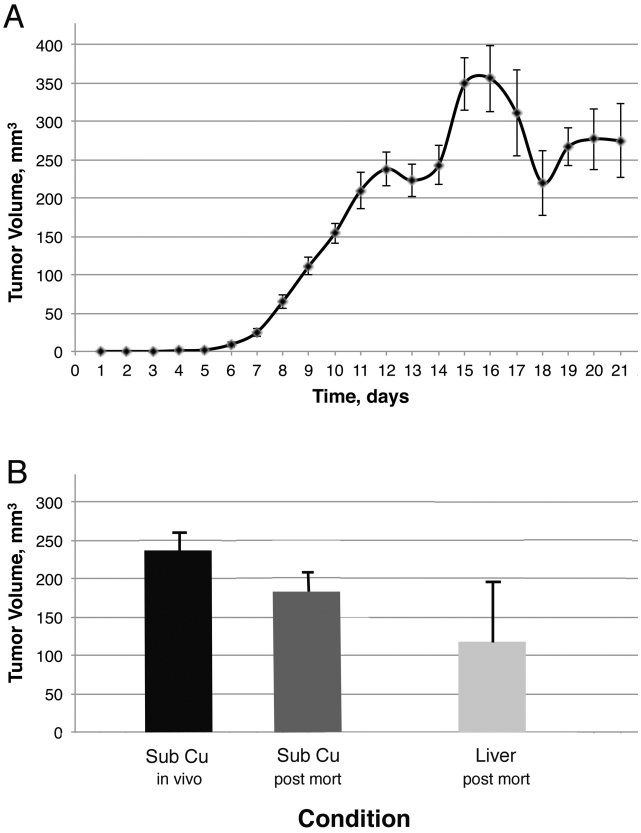

Fig. 1. Growth of Hepa 129 tumors. **A.** Calculated volumes of subcutaneous tumors over three weeks following transplantation. Means and standard error of the mean (sem) of calculated tumor volumes (using the formula: $V=4/3\ \pi\ D1/2xD2/2xD3/2$. **B.** Volumes of tumors taken from mice 12-14 days after transplantation of tumor cells. Subcutaneous tumor volumes were calculated prior to euthanasia (*in vivo*) and then measured after vascular perfusion and fixation and tumor excision. Liver tumors were measured after euthanasia by vascular perfusion.

but rather some regions display clear immunoreactivity to each of the antibodies, with other regions appearing negative.

Tumor cell genesis and expression of immunohistochemical markers

To address the question of the length of time needed for immunoreactivity to be expressed in developing tumor cells, immunohistochemical analyses was combined with systemic administration of Edu (5-ethynyl-2'-deoxyuridine), used to identify newly generated cells. Animals with tumors were euthanized at varied times following Edu administration, and the tissues processed for immunohistochemistry.

Fig. 3 presents representative tissue sections taken from animals that received systemic treatment of Edu 9 days after implantation of Hepa 129 cells, and then euthanized after an additional 1, 3, or 5 days. Sections taken through a liver tumor (Fig. 3A-C) and through a subcutaneous tumor (Fig. 3D-F) were processed for Edu (red label) and for Gly-3 (green label). These photomicrographs demonstrate that one day after Edu administration (Fig. 3A,D), the Edu labeled cells are in tumor regions that appear separate from regions that express Gly-3 immunoreactivity. At 3 days following Edu administration, the two labels continue to appear in largely separate regions of the tumor, although some overlap can be seen. By 5 days following Edu administration, the regions occupied by red Edu labeled cells are largely overlapped by regions occupied by the green Gly-3 labeled cells.

The degree of overlap between the two labeling techniques was assessed quantitatively. The areas of regions occupied by red Edu labeled cells were determined, followed by an assessment of the percent of the Edu labeled area that also was occupied by green labeled immunoreactivity. Fig. 4 presents a summary of these results, separately for intrahepatic tumors (Fig. 4B) and for subcutaneous tumors (Fig. 4A).

First, the three immunohistochemical labels were compared over the post-Edu period; analyses by ANOVA demonstrate no overall differences between the different labels ($F=0.2747$;$tp=0.9251$). Individual t-test reveals a difference only at the <3 hr time period for intrahepatic tumors ($T=2.908$; $p=0.011$). Thus the three

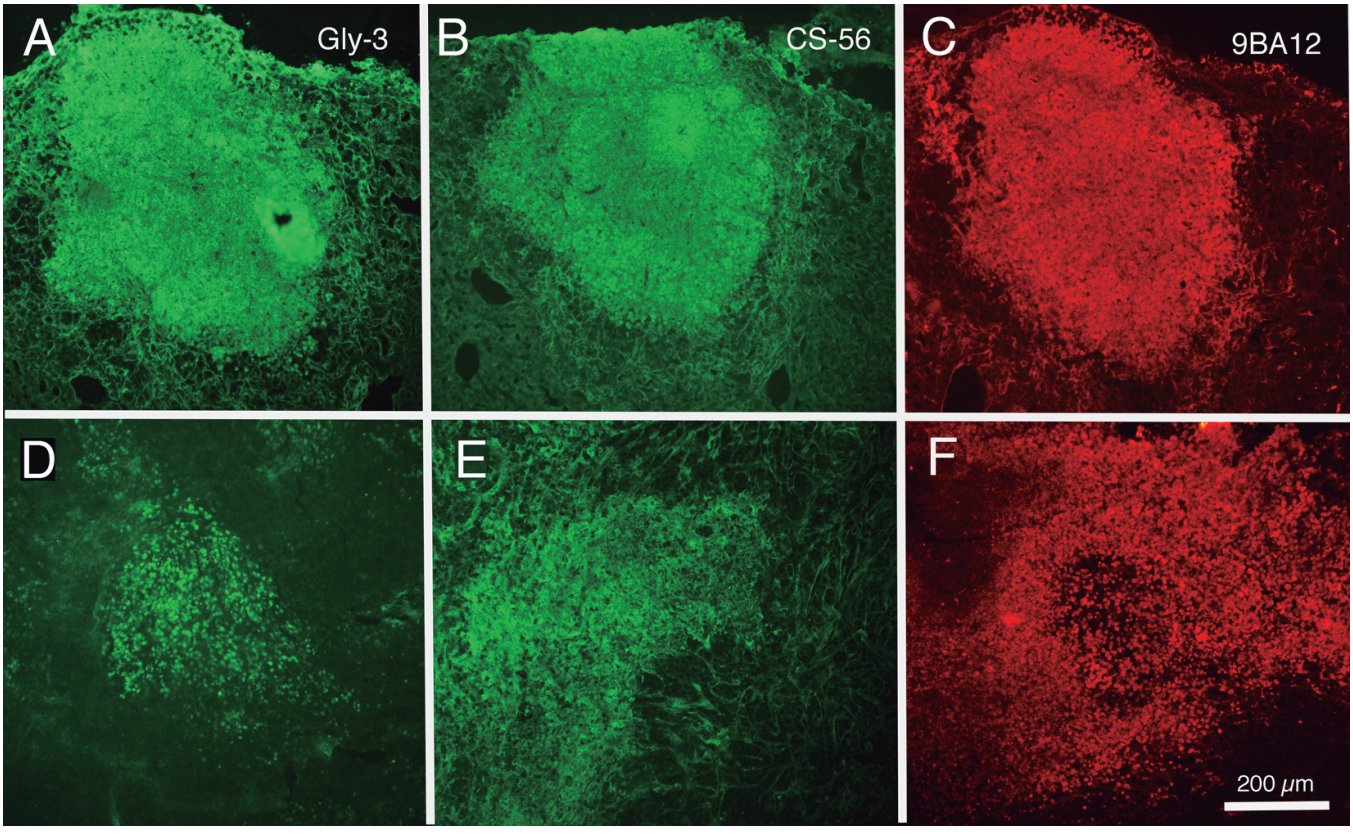

Fig. 2. Fluorescence photomicrographs showing examples of immunoreactivity of Hepa129 tumors from animals euthanized 12 days following transplantation. **A-C.** Images from sections through a Hepa 129 tumor within liver, labeled by immunoreactivity to Glypican-3 (Gly-3) **(A)**, chondroitin sulfate -56 (CS-56) **(B)**, and the 9BA12 antibody **(C)**. **D-F.** Images from sections through a subcutaneous tumor, showing immunoreactivity to the same antibodies as in **(A-C).** Scale bar: 200 μm.

labels were considered equivalent, and data were combined in further analyses.

Second, the percent overlap of the immunoreactivity and the Edu expression was found to increase significantly over the 5 day period, ($F=46.75$, $p<0.0001$). Tukey-Kramer post tests demonstrate significant differences between most of the sequential pairs of time points (asterisks in Fig. 4) for subcutaneous and for intrahepatic tumors (q values ranging from 4.658 to 8.223; $p<0.05$). The exceptions were non-significant differences for intrahepatic tumors between day 3 and day 5 ($q=2.076$; $p>0.05$) and for subcutaneous tumors between the first two time points ($q=2.412$; $p>0.05$).

Third, comparisons of intrahepatic and subcutaneous tumors over the time points examined revealed no significantly differences ($F=46.750$; $p>0.05$), as regards percent overlap of immunoreactivity and Edu labeling (q values ranging from 0.0268 to 3.825; $p>0.05$). Thus, intrahepatic and subcutaneous tumors were not different.

Vascularization of tumors

Tissues from subcutaneous and intrahepatic tumors were examined for presence of blood vessels, using immunohistochemistry and intravascular lectins to visualize the vasculature. The photomicrographs in the top row of Fig. 5 present sections of tumors from an animal euthanized 16 days after Hepa129 cell injection. Fig. 5A shows labeled vascular elements in a subcutaneous tumor, as visualized by CD31 immunoreactivity. Similarly, Fig. 5B presents another section from the subcutaneous tumor, this time showing immunoreactivity to the CD34 antibody. Fig. 5C presents a CD34 reacted section through liver tissue, showing clearly labeling of sinusoidal capillaries in regions of normal liver tissue (NL), but no apparent vascular structures within the intrahepatic Hepa129 tumor (T). Interestingly, the Hepa129 tumor cells appeared to show immunoreactivity to the CD34 antibody.

A technique was developed with the goal of specific labeling of vascular structures (Robertson et al., 2015) without concomitant labeling of tumor cells. Intravenous injections of *Lycopersicon esculentum* agglutinin (tomato lectin) lead to robust and specific labeling of vascular elements; examples are presented in the lower row of Fig. 5. For example, Fig. 5D presents a section of subcutaneous tumor, taken from a mouse that received an intravenous injection of tomato lectin 5 min prior to euthanasia by vascular perfusion. Green lectin labeling of several types of vessels is visible, including a putative arteriole (a), an accompanying venule (v), and a capillary (c). Fig. 5E presents a bright field image of another subcutaneous tumor; in this case biotinylated tomato lectin reveals several small labeled vessels (arrows). Fig. 5F presents a fluorescence photo-

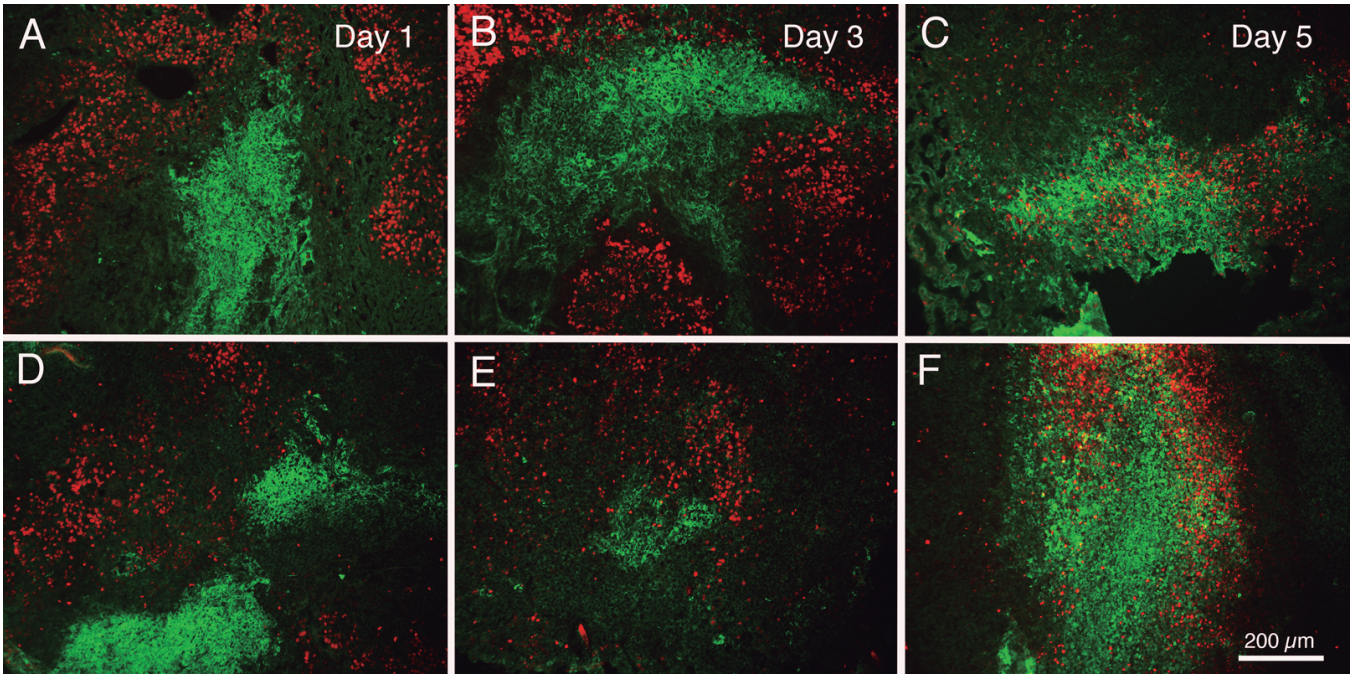

Fig. 3. Fluorescence photomicrographs of tissue sections from intrahepatic **(A-C)** and subcutaneous **(D-F)** Hepa129 tumor, from animals that received systemic treatment with Edu prior to euthanasia. Edu labeled cells are indicated by the red label, while immunoreactivity for Gly-3 is indicated by the green fluorescence. Note the distinct separation of Edu and immunoreactivity 1 day after Edu treatment, and progressively more overlap at 3 and 5 days. Scale bar: 200 μm.

micrograph showing the interface of normal liver and intrahepatic Hepa129 tumor, taken from an animal injected with Hepa129 cells 14 days prior to euthanasia. The green labeled lectin reveals the rich sinusoidal capillary network of normal liver on the right, but only very sparse labeled vessels among both the unlabeled and the red 9BA12 labeled regions of the Hepa129 tumor on the left.

Fig. 6 presents images taken from a group of littermate mice with both intrahepatic (Fig 6A,B,C) and subcutaneous (Fig. 6D,E,F) Hepa129 tumors. Animals were injected intravenously with Edu 1 day (Fig. 6A,D), 3 days (Fig. 6B,E), or 5 days (Fig. 6C,F) prior to euthanasia. Lectin was injected into the tail veins just before euthanasia. In all cases of intrahepatic tumors, the green labeled lectin reveals the rich sinusoidal capillary plexus of the liver, but only very sparse presence of labeled vessels in the Hepa129 tumor region, irrespective of length of time following Edu injection.

In contrast to the rarely encountered lectin labeled vessels in the intrahepatic tumors, labeled vessels were seen commonly in subcutaneous tumors. For example, the images presented in Fig. 6D-F were taken from subcutaneous tumors of the same mice shown in Fig. 6A-C. Fig. 6D shows labeled putative capillaries in tumor regions that either contain or do not contain Edu labled cells 1 day after Edu treatment. Fig. 6E shows large and smaller vessels in a tumor regions containing labeled cells 3 days following Edu administration, and Fig. 6F presents the same lectin label images shown in Fig. 5D, but here in the context of Edu labeled cells 5 days after Edu treatment.

Counts were made of the numbers of lectin labeled small vascular structures in subcutaneous and intrahepatic tumors, irrespective of the length or orientation of the vascular structures within the section of the tumor. Fig. 7 summarizes average numbers of small vascular structures (putative capillaries) in subcutaneous and in intrahepatic tumors, identified either by CD-31 immunohistochemistry or by intravenous lectin treatment. Results of ANOVA ($F=35.076$; $p<0.0001$) indicate significant differences. Irrespective of the technique used to identify small blood vessels, the subcutaneous tumors had significantly more vessels than did the intrahepatic tumors ($q=11.56$; $p<0.001$). The number of vessels identified by immunohistochemistry of CD-31 did not differ significantly from the number detected by intravenous lectin injection, either for subcutaneous ($q=0.743$; $p>0.05$) or for intrahepatic tumors ($q=0.664$; $p>0.05$).

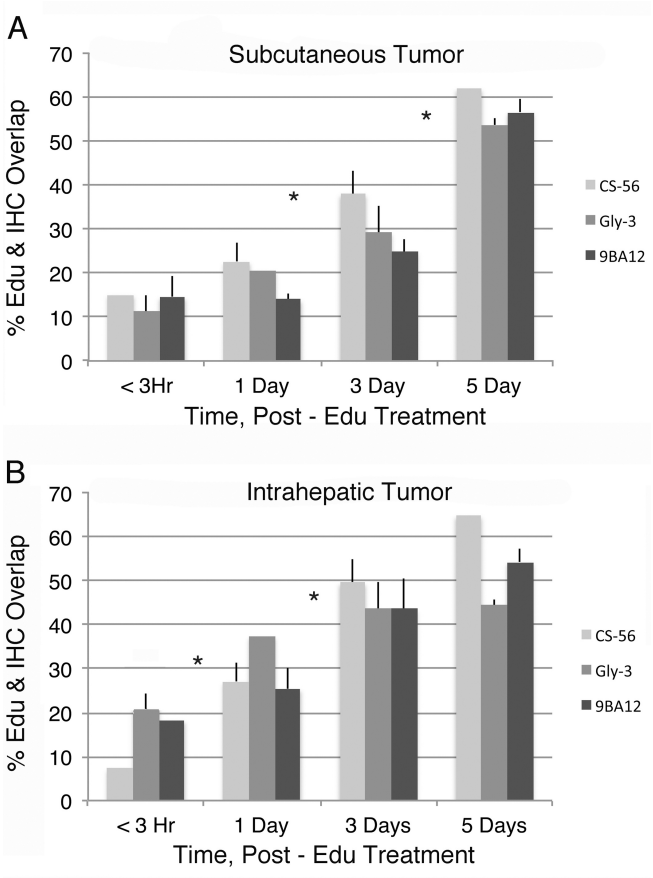

Fig. 4. Results of quantitative assessment of overlap of Edu-labeled and immunoreactive regions of Hepa129 tumors, at varied times following Edu administration. Areas of tissue sections occupied by Edu labeled cells were determined, and then the percent of those areas also displaying immunoreactivity to each of the 3 antibodies was calculated. **A.** Data (mean and sem) for subcutaneous Hepa 129 tumors. **B.** Data for intrahepatic Hepa 129 tumors. Histograms without error bars indicate data from fewer than 3 cases. The asterisk indicate significant increases in degree of overlap between subsequent time periods.

Discussion

Selection of a tumor model

Several tumor models are available for basic science research, each with strengths and weaknesses (Newell et al., 2008; Heindryckx et al., 2009; Fausto and Campbell, 2010; Shiraha et al., 2013). The Hepa129 syngeneic tumor cell line (Schmitz et al., 2004) was derived from mouse hepatoma and was chosen for these studies because it produces either ectopic subcutaneous tumors or orthotopic intrahepatic tumors, and offers the advantage of a short time span between cell injection and tumor development. This Hepa129 tumor model has demonstrated its utility through studies by Schmitz and colleagues (Raskopf et al., 2005, 2008) and by other investigators (Schmieder et al., 2013; Piccioni et al., 2015).

The present studies indicate similar growth rates and similar immunohistochemical profiles in subcutaneous and intrahepatic tumors. Li et al. (2012) suggest that orthotopic tumors in the liver are the preferred choice because they better mimic clinical conditions, including tumor location, accompanying liver damage, and the interaction of tumor cells with the liver micro-

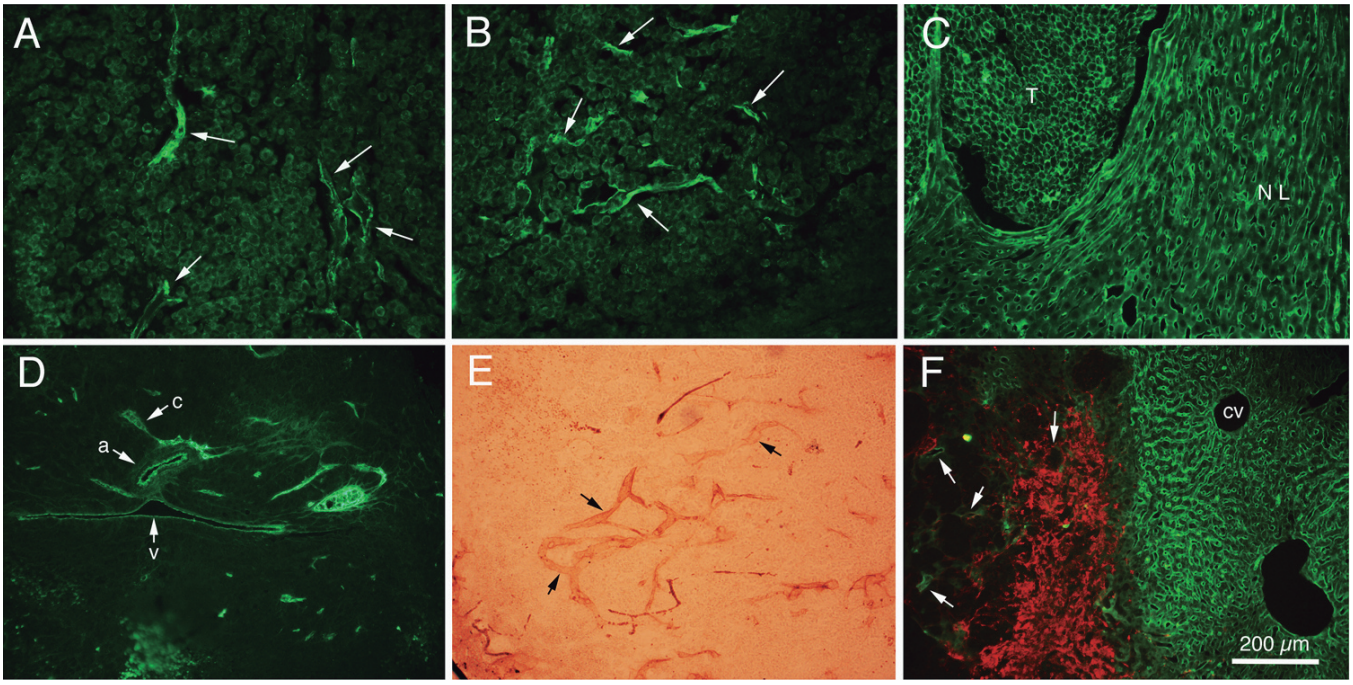

Fig. 5. Labeling vascular structures in Hepa 129 tumors. **A.** Fluorescence photomicrograph showing green CD-31 labeled vascular structures (arrows) in a section of subcutaneous Hepa129 tumor. **B.** Green CD-34 labeled vascular structures (arrows) in another subcutaneous Hepa129 tumor. **C.** Green CD-34 labeling of sinusoidal capillaries in normal liver (NL) tissue. No vascular structures are apparent in the tumor (T) nodule, although CD-34 immunoreactivity appears around tumor cells. **D.** Green tomato lectin labeled vascular structures in a subcutaneous Hepa 129 tumor. The lectin labels the endothelial cell lining of a probable arteriole (a), a capillary (c), and a venule (v). (This image also is included as part of Fig. 6F). **E.** Brightfield photomicrograph of a biotin processed section from a subcutaneous Hepa129 tumor. Arrows indicate labeled vessels. **F.** Fluorescence micrograph showing the interface of normal liver, on right, and 9BA12 labeled Hepa129 tumor, on left. The green lectin shows the rich sinusoidal capillary network of the normal liver, but very few labeled vessels (arrows) in the red 9BA12 labeled tumor. Scale bar: 200 μm.

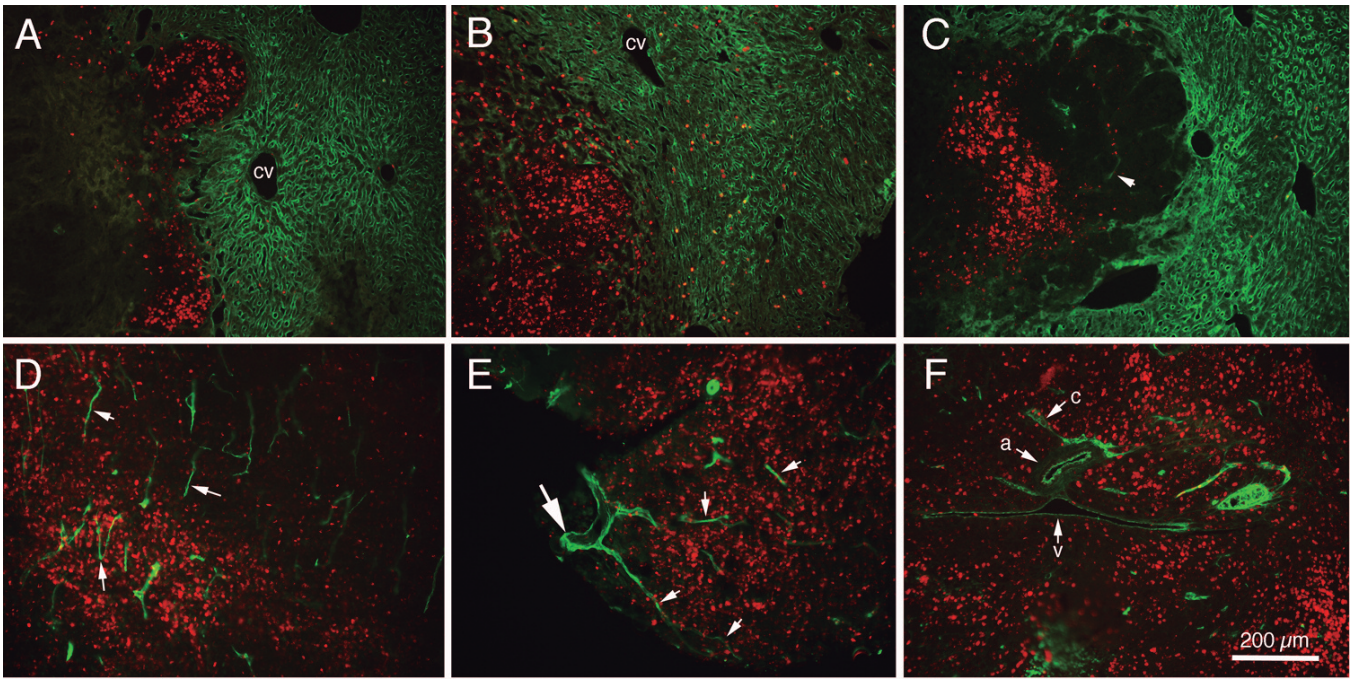

Fig. 6. Vascular structures in intrahepatic and in subcutaneous Hepa 129 tumors. **A-C.** Fluorescence micrographs of intrahepatic Hepa129 tumor, showing green lectin labeled vasculature and red Edu labeled cells of liver tumors at 1 day **(A)**, 3 days **(B)**, and 5 days **(C)** following Edu injections. Lectin labeled blood vessels in the tumor region are very sparse (arrow) or absent. **D-F.** Fluorescence micrographs showing green lectin labeled vasculature and red Edu labeled cells of subcutaeneous Hepa129 tumors at 1 day **(D)**, 3 days **(E)**, and 5 days **(F)** after Edu injections. Vascular structures are more common in subcutaneous tumor tissue, and include probable capillaries (small arrows in **D and E**; c in **F**), arteriole (a in **F**), venule (v in **F**). cv: central venule. Scale bar: 200 μm.

environment.

However, implantation of syngeneic tumor cell lines may not produce ideal model systems. A surprising finding was the relatively poor vascularization of the intrahepatic tumors, whereas human HCC reportedly is highly vascularized, with most stemming from the hepatic artery rather than portal vein (Cazejust et al., 2014). Further, human HCC usually occurs in combination with and partially resulting from cirrhosis, infections (either hepatitis B or C), or chronic ethanol consumption (Johnson, 1997; Llovet et al., 2003). Thus, a better mouse model may include liver damage as a precedent to HCC.

Tumor growth and metastasis

The present data indicate that both subcutaneous and intrahepatic tumors grew in size over the 2 weeks following implantation, but that subcutaneous tumors had greater volume. It is not clear why the subcutaneous tumors attained greater volume, although the greater vascularization of subcutaneous tumors may be important. The growth data support and extend the results of Schmitz et al. (2004), who used ultrasound measurements *in vivo* followed by direct measurements of tumors during surgical exploration, and report data similar to those described here. The use of ultrasound measurements (Schmitz et al., 2004) offers clear and obvious advantages for following tumor growth, and possibly tumor regression from treatment over time.

Tumor metastasis can accompany growth. Other investigators have reported evidence of metastatic tumors in lungs of mice (Li et al., 2012), and that metastasis is more likely to occur from intrahepatic than from subcutaneous sites (Leenders et al., 2008). The present experiments revealed no evidence of tumor metastasis from either the subcutaneous or intrahepatic tumors, although these short-term studies may not have allowed sufficient time for migration of tumor cells and/or development of metastatic tumors of sufficient size to be detected.

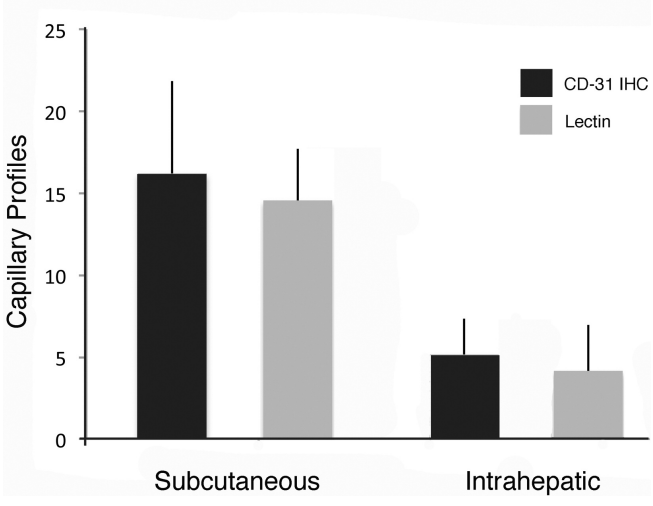

Fig. 7. Numbers of capillary profiles in tissue sections from subcutaneous and intrahepatic Hepa129 tumors. Means and standard deviations (error bars) are given for capillaries identified by CD-31 immunohistochemistry or by intravenous lectin administration.

Differentiation of tumor cells

Several markers have been used to identify hepatocellular carcinoma, including alpha-fetoprotein (Korn, 2001), laminin-5, and intercellular adhesion molecule-1 (Qin and Tang, 2004). Many tumor types, including HCC, exhibit specific changes in glycosaminoglycan and proteoglycan expression compared to normal tissue (Kojima et al., 1975; Kovalszky et al., 1993; Lv et al., 2007; Iozzo and Sanderson, 2011; Svensson et al., 2011; Afratis et al., 2012; Jia et al., 2013). Because of their ability to bind multiple growth factors, extracellular glycosaminoglycans have been proposed to be important co-receptors for signaling pathways that promote tumor progression, and hence the glyocosaminoglycans could provide a good marker for growing tumors (Kojima et al., 1975; Kovalszky et al., 1993; Lv et al., 2007; Iozzo and Sanderson, 2011; Svensson et al., 2011; Arfatis et al., 2012; Jia et al., 2013) .

Glypican-3, or heparan sulfate proteoglycan, is a 770 kd protein and member of the glypican family. It is currently viewed as a reliable clinical marker of HCC in humans (Filmus and Capurro, 2013), as this proteoglycan is not detected in normal adult liver, cirrhotic liver, or in other non-malignant lesions. Heparan sulfate has been demonstrated in the endothelium and space of Disse of normal mouse liver and can be targeted by peptide-containing liposomes (Longmuir et al., 2006; 2009; Robertson et al., 2008). Clinical investigations are currently in progress to treat HCC by immunologic inhibition of glypican-3 expression or function (Zhu et al., 2001; Allegetta and Filmus, 2011; Filmus and Capurro, 2013; Feng and Ho, 2014), hence it is important to document the expression of this proteoglycan in tumor cell lines used in HCC research. In the present study, both intrahepatic and subcutaneous Hepa129 tumor cells expressed Gly-3.

The chondroitin sulfate class of proteoglycans also shows significant changes in expression during tumor development (Lv et al., 2007; Svensson et al., 2011; Jia et al., 2013). Lv et al. (2007) reported that chondroitin sulfate levels were significantly higher in human samples of HCC, with the highest levels associated with the more advanced cases. Normal liver contains low levels of chondroitin sulfate, and chondroitin sulfate is absent from the sinusoidal regions (Robertson et al., 2008; Jia et al., 2013). Immunohistochemical labeling with both the CS-56 monoclonal antibody and the 9BA12 antibody were quite similar in both ectopic and orthotopic tumors, and both labels revealed marked

differences between the tumor and adjacent normal liver tissue in the intrahepatic tumors.

Tumor regions containing recently generated cells *in vivo*, as defined as positively labeled a few hours following Edu administration, do not express detectable levels of immunoreactivity to any of the antibodies used. Only after a few days do the regions of Edu labeling overlap with regions displaying immunoreactivity to the antibodies. These results suggest that maturation of the newly generated tumor cells, perhaps involving stimulation by as yet unknown factors in the local environment, is required for the expression of these tumor-specific markers.

Ingrowth of vascular elements

Ingrowth of new vasculature is widely considered as being essential for tumor growth, and therefore a great deal of effort is being directed toward understanding the neovascularization of tumors and of using anti-angiogenic approaches to limit tumor growth (Folkman, 1971; Eliceiri and Chesresh, 2001; Raskopf et al., 2008; Zhu et al., 2011). Results from the present study indicate that growth of blood vessels is relatively robust in the subcutaneous tumors, but significantly less so in the intrahepatic tumors. The reason for this difference between the vasculature of ectopic and orthotopic tumors is not clear at present, but possibilities include that subcutaneous tissue in general is relatively poorly vascularized, and ingrowth of new vessels may be required for tumor growth and survival. In contrast, the normal liver is highly vascularized by a discontinuous and fenestrated capillary bed (Baratta et al., 2009) and perhaps the growing tumor cells receive sufficient access to nutrients and oxygen from leakage through this existing porous vasculature and formation of new capillaries may not be needed. The present demonstration of rather few vascular elements in the orthotopic Hepa129 tumors is in agreement other recent reports of rather few CD31 (or PECAM-1) positive vessels in a mouse model of HCC, although adjacent normal liver vasculature is clearly positive (Piccioni et al, 2015). Interestingly, even though vascular elements appear rare in these tumors, reductions in vascular endothelial growth factor (VEGF, a known promoter of vascularization in tumors and normal tissue) was shown to reduce tumor size (Piccioni et al., 2015). Because vascular endothelial growth factor (VEGF) is important for angiogenesis (Eliceiri and Chesresh, 2001; Raskopf et al., 2008) a search for VEGF levels in ectopic and orthotopic tumor sites and environments would be of great interest.

Human hepatocellular carcinoma is known to be highly vascularized (Tanigawa et al., 1997; Coulon et al., 2011) and angiogenesis is considered to be essential for HCC development, progression and metastasis (Coulon et al., 2011). In this context, an understanding of angiogenesis may be vitally important in development of an effective therapy. Thus, the orthotopic Hepa129 tumors may not provide the best model system in pursuit of this goal.

Conclusions

The syngeneic Hepa129 tumor in the C3H mouse, including both ectopic and orthotopic tumors, appears useful for studies of development and differentiation of proteoglycan and glycosaminoglycan expression relevant to hepatocellular carcinoma in humans. If these proteoglycan markers are used as targets for drug delivery systems, it must be considered that newly formed tumor cells do not display the targeted molecules until at least 2 days after cell production. In regard to attempts to inhibit angiogenesis as a treatment to prevent metastasis and growth of tumors, the orthotopic intrahepatic tumors may be less useful than ectopic subcutaneous tumors in this model system.

Acknowledgements. This work was supported by University of California Cancer Research Coordinating Committee grant to RTR, and by NIH Award P30CA062203 to the University of California, Irvine, Chao Family Comprehensive Cancer Center.

References

Afratis N., Gialeli C., Nikitovic D., Tsegenidis T., Karousou E., Theocharis A.D., Pavao M.S., Tzanakakis G.N. and Karamanos N.K. (2012). Glycosaminoglycans: key players in cancer cell biology and treatment. FEBS J. 279, 1177-1197.

Allegretta M. and Filmus J. (2011). Therapeutic potential of targeting glypican-3 in hepatocellular carcinoma. Anticancer Agents Med. Chem. 11, 543-548.

Bakiri L. and Wagner E.F. (2013). Mouse models for liver cancer. Mol. Oncol. 7, 206-233.

Baratta J.L., Ngo A., Lopez B., Kasabwala N., Longmuir K.J. and Robertson R.T. (2009). Cellular organization of normal mouse liver: a histological, quantitative immunocytochemical, and fine structural analysis. Histochem. Cell Biol. 131, 713-726.

Cazejust J., Bessoud B., Colignon N., Garcia-Alba C., Planche O. and Menu Y. (2014). Hepatocellular carcinoma vascularization: from the most common to the lesser known arteries. Diagn. Interv. Imag. 95, 27-36.

Coulon S., Heindryckx F., Geerts A., Van Steenkiste C., Colle I. and Van Vliergerghe H. (2011). Angiogenesis in chronic liver disease and its complications. Liver Int., 31, 146-162.

DeMincis S., Kisseleva T., Francis H., Baroni G.S., Benedetti A., Brenner D., Alvaro, D, Alpini G. and Marzioni M. (2013). Liver carcinogenesis: rodent models of hepatocarcinoma and cholangiocarcinoma. Dig. Liver Dis. 45, 450-459.

Eliceiri B.P. and Chesresh D.A. (2001). Adhesion events in angiogenesis. Curr. Opin. Cell Biol. 13, 563-568.

Fausto N. and Campbell J.S. (2010). Mouse models of hepatocellular carcinoma. Seminars Liver Dis. 30, 87-98.

Feng M. and Ho M. (2014). Glypican-3 antibodies: a new therapeutic target for liver cancer. FEBS Lett. 588, 377-382.

Filmus J. and Capurro M. (2013). Glypican-3: a marker and a therapeutic target in hepatocellular carcinoma. FEBS J. 280, 2471-

2476.

Folkman J. (1971). Tumor angiogenesis: therapeutic implications. N. Engl. J. Med., 285, 1182-1186.

Forner A., Llovet J.M. and Bruix J. (2012). Hepatocellular carcinoma. Lancet 379, 1245-1255.

Heindryckx F., Colle I. and Van Vlierberghe H. (2009). Experimental mouse models for hepatocellular carcinoma research. Int. J. Exp. Path. 90, 367-386.

Iozzo R.V. and Sanderson R.D. (2011). Proteoglycans in cancer biology, tumour microenvironment and angiogenesis. J. Cell Mol. Med. 15, 1013-1031.

Jia X.L., Li S.Y., Dang S.S., Cheng Y.A., Zhang X., Wang W.J., Hughes C.E. and Caterson B. (2013). Increased expression of chondroitin sulphate proteoglycans in rat hepatocellular carcinoma tissues. World J. Gastroenterol. 18, 3962-3976.

Johnson R.C. (1997). Hepatocellular carcinoma. Hepatogastroenterology 44, 37-312.

Khaled W.T. and Liu P. (2014). Cancer mouse models: past, present and future. Sem. Cell Dev. Biol. 27, 5-60.

Kojima J., Nakamura N., Kanatani M. and Omori K. (1975). The glycosaminoglycans in human hepatic cancer. Cancer Res. 35, 542-547.

Korn W.M. (2001). Moving toward an understanding of the metastatic process in hepatocellular carcinoma. World J. Gastroenterol. 7, 777-778.

Kovalszky I., Schaff Z., and Jeney A. (1993). Potential markers (enzymes, proteoglycans) for human liver tumors. Acta Biomed. Ateneo Parmense. 64, 157-163.

Leenders M.W.H., Nijkamp M.W. and Rinkes I.H.M.B. (2008). Mouse models in liver cancer research: a review of current literature. World J. Gastroent. 14, 6915-6923.

Li Y., Tang Z-Y, Hou J-X. (2012). Hepatocellular carcinoma: insight from animal models. Nature Rev. Gastroent. Hepatol., 9, 32-43.

Llovet J.M., Burroughs A., and Bruix J. (2003). Hepatocellular carcinoma. Lancet 362, 1907-1917.

Longmuir K.J., Robertson, R.T., Haynes S.M., Baratta J.L. and Waring A.J. (2006). Effective targeting of liposomes to liver and hepatocytes *in vivo* by incorporation of a Plasmodium amino acid sequence. Pharmaceut. Res. 23, 759-769.

Longmuir K.J., Haynes, S.M., JBaratta J., Kasabwala N, and Robertson R.T. (2009). Liposomal delivery of doxorubicin to liver and hepatocytes *in vivo* by targeting hepatic heparan sulfate glycosaminoglycan, Int. J. Pharmaceut. 382, 222-233.

Lv H., Yu G., Sun L., Zhang Z., Zhao X. and Chai W. (2007). Elevated level of glycosaminoglycans and altered sulfation pattern of chondroitin sulfate are associated with differentiation status and histological type of human primary hepatic carcinoma. Oncology 72, 347-356.

Newell P., Villanueva A., Friedman S.L., Koike K. and Llovet J.M. (2008). Experimental models of heptocelllular carcinoma. J. Hepatol. 48, 858-879.

Qin L.X. and Tang Z.Y. (2004). Recent progress in predictive biomarkers for metastatic recurrence of human hepatocellular carcinoma: a review of the literature. J. Cancer Res. Clin. Oncol. 130, 497-513.

Piccioni F., Fiore E., Bayo J., Atorrasagasti C., Peixoto E., Rizzo M., Malvicini M., Tirado-Gonzalez I., Garcia M.G., Alaniz L. and Mazzollni G. (2015). 4-methylumbelliferone inhibits hepatocelluar carcinoma growth by decreasing IL-6 production and angiogenesis. Glyocobiology 25, 825-835.

Raskopf E., Dzienisowicz C., Hilbert T., Rabe C., Leifeld L., Wernert N., Sauerbruch T., Prieto J., Qian C., Caselmann W.H. and Schmitz V. (2005). Effective angiostatic treatment in a murine metastatic and orthotopic hepatoma model. Hepatology 41, 1233-1240.

Raskopf E., Vogt A., Sauerbruch T. and Schmitz V. (2008). siRNA targeting VEGF inhibits hepatocellular carcinoma growth and tumor angiogenesis *in vivo*. J. Hepatol. 49, 977-984.

Robertson R.T., Baratta J., Haynes S.M. and Longmuir K.J. (2008). Liposomes incorporating a Plasmodium amino acid sequence target heparan sulfate biding sites in liver. J. Pharm. Sci. 97, 3257-3273.

Robertson R.T., Levine S.T., Haynes S.M., Gutierrez P., Baratta J.L., Tan Z. and Longmuir K.J. (2015). Use of labeled tomato lectin for imaging vascular structures. Histochem. Cell Biol. 143, 225-234.

Schmieder R., Puehler F., Neuhaus R., Kissel M., Adjei A.A., Miner J.N, Mumberg D., Ziegelbauer K. and Scholz A. (2013). Allosteric MEK1/2 inhibitor Refametinib (BAY 86-9766) in combination with Sorafenib exhibits antitumor activity in preclinical murine and rat models of hepatocellular carcinoma. Neoplasia 15, 1161-1171.

Schmitz V., Tirado-Ledo L., Tiemann K., Raskopf E., Heinicke T., Ziske C. Gonzalez-Carmona M.A., Rabe C., Wernert N., Prieto J., Qian C., Sauerbruch, T. and Caselmann W.H. (2004). Establishment of an orthotopic tumour model for hepatocellular carcinoma and non-invasive *in vivo* tumour imaging by high resolution ultrasound in mice. J. Hepatol. 40, 787-791.

Shiraha H., Yamamoto K. and Namba M. (2013). Human hepatocyte carcinogenesis (review). Int. J. Oncol. 42, 1133-1138.

Svensson K.J., Christianson H.C., Kucharzewska P., Fagerström V., Lundstedt L., Borgquist S. Jirström K and Belting M. (2011). Chondroitin sulfate expression predicts poor outcome in breast cancer. Int. J. Oncol. 39, 1421-1428.

Tanigawa N., Lu C., Mitsui T. and Mimura S. (1997). Quantitation of sinusoidal-like vessels in hepatocellular carcinoma: its clinical and prognostic significance. Hepatology 26, 1216-1223.

Yang R., Rescorla F.J., Reilly C.R., Faught P.R., Sanghvi N.T, Lumeng L. Franklin T.D. Jr. and Grosfeld J.L. (1992). A reproducible rat liver cancer model for experimental therapy: introducing a technique of intrahepatic tumor implantation. J. Surg. Res. 52, 193-198.

Zhu Z.-W., Friess H., Wang L., Abou-Shady M., Zimmermann A., Lander AD, Korc M, Kleeff J. and Büchler M.W. (2001). Enhanced glypican-3 expression differentiates the majority of hepatocellular carcinomas from benign hepatic disorders. Gut 48, 558-564.

Zhu A.X., Dusa D.G., Sahani D.V. and Jain R.K. (2011). HCC and angiogenesis: Possible targets and future directions. Nat. Rev. Clin. Oncol. 8, 292-301.

Accepted November 9, 2015